CORROSION SCIENCE AND TECHNOLOGY, Vol.9, No.2(2010), pp.81~86

CMnAl TRIP Steel Surface Modification During CGL Processing

Y. F. Gong, Y. R. Lee, Han S. Kim, and B. C. De Cooman†

Materials Design Laboratory, Graduate Institute of Ferrous Technology, Pohang University of Science and Technology, Pohang, South Korea
(Received August 3, 2009; No Revision; Accepted March 28, 2010)

The mechanisms of selective oxidation of intercritically annealed CMnAl TRIP steels in a Continuous Galvanizing Line (GCL) were studied by cross-sectional observation of the surface and sub-surface regions by means of High Resolution Transmission Electron Microscopy (HR-TEM). The selective oxidation and nitriding of an intercritically annealed CMnAl TRIP steel in a controlled dew point 10%H_2+N_2 atmosphere resulted in the formation of *c*-x$MnO.MnO_2$ ($1 \leq x < 3$) and *c*-x$MnO.Al_2O_3$ ($x \geq 1$) particles on the steel surface. Single crystal *c*-x$MnO.SiO_2$ ($2 \leq x \leq 4$) oxide particles were also observed on the surface. A thin film of crystalline *c*-x$MnO.SiO_2$ ($2 \leq x < 3$) and *c*-x$MnO.Al_2O_3$ ($x \geq 1$) was present between these particles. In the sub-surface region, internal oxidation, nitriding and intermetallic compound formation were observed. In the first region, large crystalline *c*-x$MnO.SiO_2$ ($1 \leq x \leq 2$) and *c*-x$MnO.Al_2O_3$ ($x \geq 1$) oxides particles were present. In the second region, c-AlN particles were observed, and in a third region, small $MnAl_x$ ($x>1$) intermetallic compound particles were observed.

Keywords *: oxidation, TRIP steel, CGL, intermetallic compound, HR-TEM*

1. Introduction

Multi-phase TRIP steel is ideally suited for structural parts of car bodies which are specifically related to the passive passenger safety during frontal collisions. This is due to the high strain rate energy absorption potential of TRIP steel. Automotive TRIP steels are usually galvanized to ensure an adequate perforation corrosion resistance. A high Si content is a key feature of standard TRIP steel compositions, as Si is effective in suppressing the carbide formation during the bainite transformation. It is well known that standard TRIP steels alloyed with high Si contents cannot be processed in conventional continuous galvanizing lines (CGL) due to the formation of surface defects related to the selective oxidation of Si. This has led to the development of low Si and Si-free, Al-alloyed TRIP steel compositions which are compatible with CGL processing. The fundamental reason for the improved galvanizing performance of the Al-alloyed TRIP steels is still not understood as the selective oxidation of Al is also expected. The gas atmosphere of the industrial annealing furnace in continuous hot dip galvanizing lines (HDG) leads to the reduction of the iron oxides formed during cold rolling. It also results in the selective oxidation of the key alloying additions of Si, Mn and Al. The presence of film-forming surface oxides is believed to deteriorate the wettability of the steel by molten Zn and prevent the formation of the $Fe_2Al_{5-x}Zn_x$ inhibition layer.[1),2)] Research on improving the galvanizability of Si-bearing TRIP steel by replacing Si with Al has been studied for several years.[2)-6)] The external oxides on the surface and the internal oxides in the sub-surface have been studied previously by Scanning Electron Microscopy (SEM), X-ray Photo-electron Spectroscopy (XPS), Secondary Ion Mass Spectroscopy (SIMS), Energy Dispersive Spectrometry (EDS) and Glow Discharge Optical Emission Spectroscopy (GDOES).[3),4),7),8),13)] The direct observation of the morphology, size, distribution and composition of internal and external oxides on intercritically annealed CMnAl TRIP steel has not yet been reported. High Resolution Transmission Electron Microscopy (HR-TEM) of Focused Ion Beam (FIB) cross-sectional samples was therefore used to carry out an in-depth analysis of the composition and micro-structure of the external and internal oxidation of CMnAl TRIP steel during intercritical annealing.

† Corresponding author: decooman@postech.ac.kr

2. Experimental

The starting material used in the present work was full hard cold rolled CMnAl TRIP steel. The composition was 0.158 mass% C, 1.99 mass% Mn, 1.01 mass% Al and 0.31 mass% Si. The sample surface was mirror-polished with a diamond suspension prior to annealing in order to avoid all effects related to the roughness of the strip surface. The thermal cycle was carried out in a furnace with a controlled 10%H_2+N_2 atmosphere with a dew point of -25 ℃. The intercritical annealing temperature was 827 ℃ and the soaking time was 120 seconds. The heating rate was +5 ℃/min. The sample was quenched from the intercritical temperature to room temperature by high purity He in a quenching chamber. The annealed samples were investigated in a JEOL JEM-2100F TEM equipped with a field-effect electron source. The cross-sectional samples prepared by FIB allowed for the analysis of composition, crystal structure, morphology, size, spatial distribution and interfacial structure of the oxides on the steel surface and in the sub-surface region. The determination of the oxide composition was done by means of Energy Dispersive Spectroscopy (EDS).

3. Results

A typical cross-sectional view of the surface and sub-surface regions for an intercritically annealed sample is shown in Fig. 1. Oxides were present at the surface as either larger particles (zone A) or as thin films (zone B). The surface areas covered with the larger oxide particles are clearly separated from the areas where the oxide is present as a thin film. The black layer on the surface oxides is a protective Au coating layer deposited on the sample surface prior to the FIB sample preparation. Three distinct zones were observed in the sub-surface. The first zone was ~730 nm below the surface. Oxide networks and separate inter-granular oxides particles with a diameter of 50-170 nm were observed in this zone.

The second zone was in the range of 0.73-1.63 μm below the surface. Small nitrides were observed in this second zone. In the range of 1.63-4.0 μm below surface, intermetallic compound particles were observed. No martensite was found after quenching in the sub-surface region in the range of 0-4 μm below the surface. Fig. 2 shows a cross sectional view of the surface oxides. The larger oxide particles are about 47 nm in diameter. Fig. 2b is a detail of the $xMnO.SiO_2$ ($1 \leq x < 3$), $xMnO.Al_2O_3$ ($x \geq 1$) and $xMnO.SiO_2$ ($2 \leq x \leq 4$) particles in area A on the surface. The lattice image for the $xMnO.SiO_2$ ($2 \leq x \leq 4$) oxide is shown in Fig. 2c.

Fig. 2d shows the large crystalline *c*-$xMnO.SiO_2$ ($1 \leq x < 3$) and *c*-$xMnO.Al_2O_3$ ($x \geq 1$) oxide particles. The interface between the oxides and matrix is indicated in the

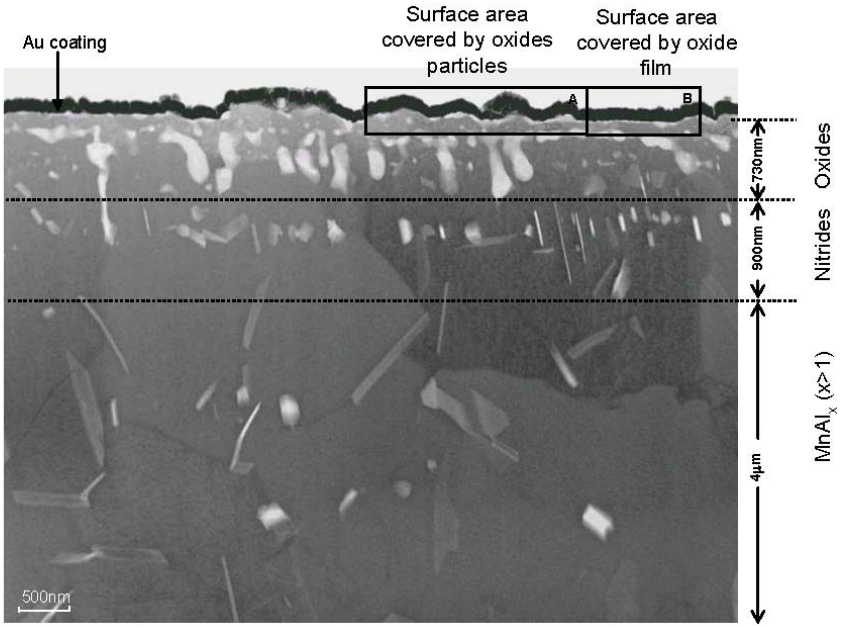

Fig. 1. Overview TEM cross-sectional micrograph of the surface and sub-surface for CMnAl TRIP steel annealed at an intercritical temperature of 827 ℃ in a 10%H_2+N_2 gas atmosphere with a dew point of -25 ℃. The black layer on the surface oxides is a protective Au coating. Oxides particles (zone A) and a thin oxide film (zone B) are observed on the original steel surface. In the sub-surface, internal oxides, nitrides and intermetallic compounds form three distinct regions.

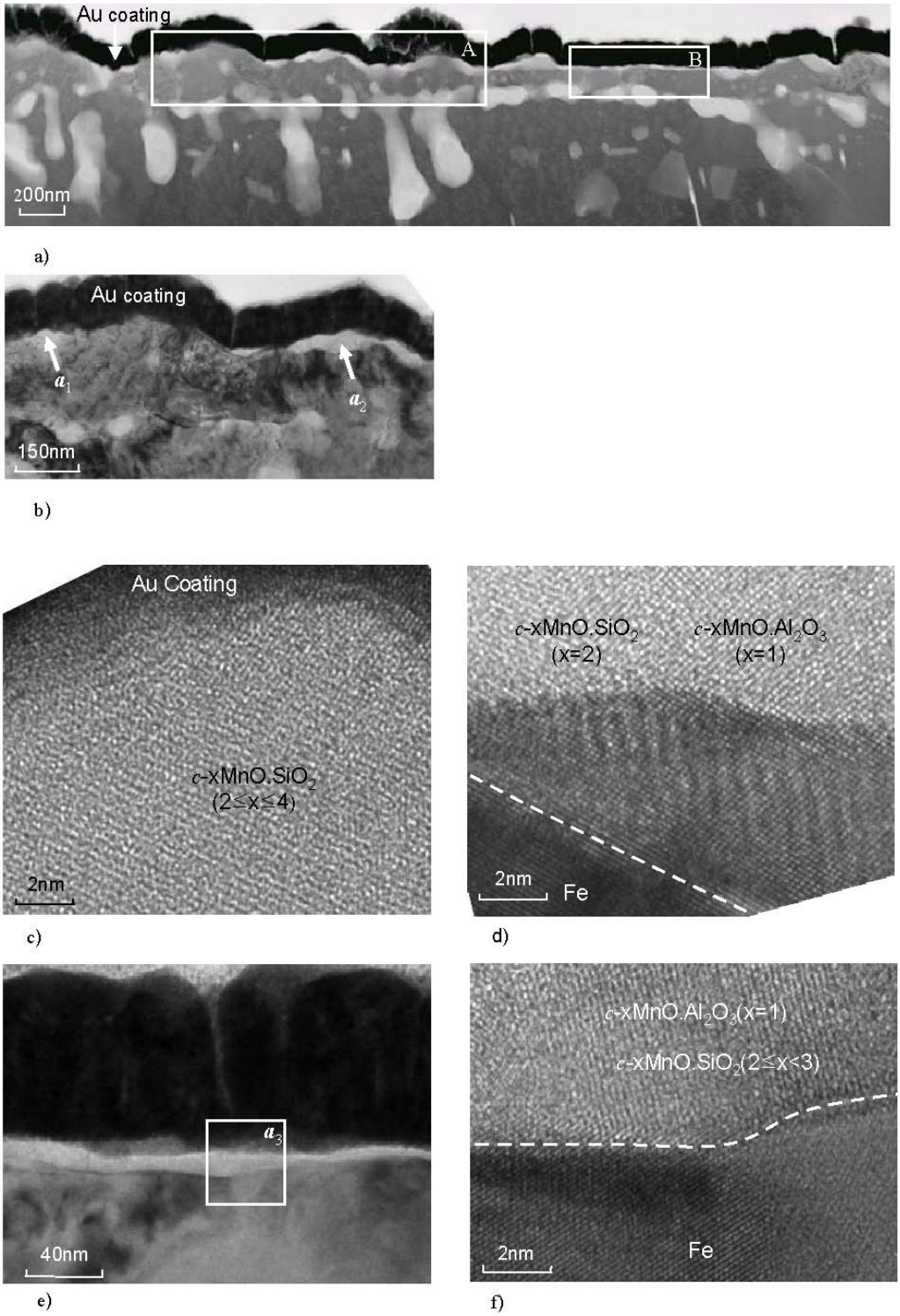

Fig. 2. Cross-sectional TEM micrographs for the CMnAl TRIP steel with surface covered with $xMnOSiO_2$ ($2 \leq x \leq 4$) and $xMnO.Al_2O_3$ (x=1) oxide particles and a $xMnO.SiO_2$($2 \leq x < 3$) and $xMnO.Al_2O_3$(x=1) oxide film. (a) Overview of the surface area covered with large $xMnO.SiO_2$ and $xMnO.Al_2O_3$ oxides particles and thin oxides film. (b) Detailed micrographs corresponding to zone A in a, showing the large oxides particles. (c) Micrograph of *c*-$xMnO.SiO_2$ with $2 \leq x \leq 4$ (arrow a_1 in b). (d) Interface (dotted white line) between the *c*-$MnO.SiO_2$ (x=2) and *c*-$xMnO.Al_2O_3$ (x=1) oxides particles and the matrix (arrow a_2 in b). (e) Micrographs corresponding to zone B in a, showing the thin oxides film. (f) Interface (dotted white line) of the thin film of *c*-$xMnO.SiO_2$ ($2 \leq x < 3$) and *c*-$xMnO.Al_2O_3$ (x=1) oxides and the matrix (zone a_3 in e).

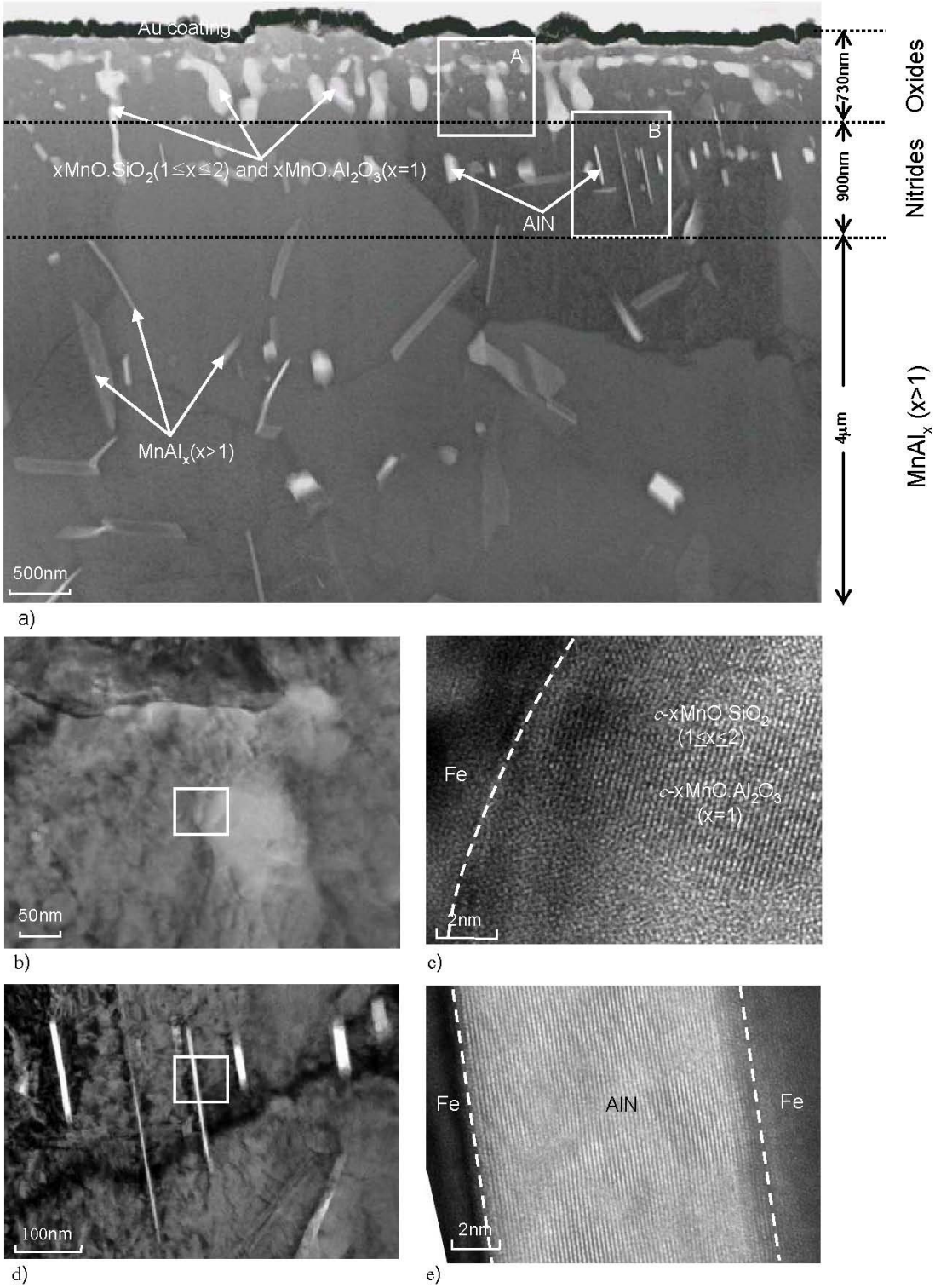

Fig. 3. Cross-sectional TEM micrographs for the three sub-surface zones. Zone I contains larger *c*-xMnO.SiO_2 ($1x\leq 2$) and *c*-xMnO.Al_2O_3 (x=1) particles, Zone II contains small AlN particles and Zone III has $MnAl_x$ (x>1) intermetallic particles. (a) Overview of the three zones. (b) Detailed micrograph of zone A in (a). (c) Micrograph of *c*-xMnO.SiO_2 ($1\leq x2$) and *c*-xMnO.Al_2O_3 (x=1) oxides particle in (b). The white dotted line indicates the position of the interface between the matrix and the oxides. (d) Detailed micrograph of zone B in (a). (e) Lattice image of AlN in (d). The dotted white line indicates the position of the interface between the matrix and the nitride.

lattice image by means of the dotted white line. The observations are in agreement with those reported by Mahieu *et al.*[2] and Bellhouse *et al.*[6]. Fig. 2e shows the thin crystalline oxide film on the surface, visible on the right hand side of the micrograph in Fig. 1. A detailed micrograph of this surface film is shown in Fig. 2f, which also indicates the position of the interface between the crystalline oxide film and the steel matrix in zone a_3 of Fig. 2e. EDS analysis revealed that this film-type oxide consisted of the crystalline oxides *c*-xMnO.SiO_2 ($2 \leq x < 3$) and *c*-xMnO.Al_2O_3 ($x \sim 1$).

There are three distinct zones in the sub-surface, as shown in Fig. 3a. The first zone is the internal oxidation zone in the range of approximately 730 nm below the surface. Large inter-granular crystalline oxide particles with a diameter in the range of 50-170 nm were observed in this zone. The detailed structure of the oxide particles in this zone is shown in the micrograph of Fig. 3b. These particles were identified as the crystalline oxides *c*-xMnO.SiO_2 ($1 \leq x \leq 2$) and *c*-xMnO.Al_2O_3(x=1).

Fig. 3c shows the interface between these oxides and the matrix. Fig. 3d shows the structure of the second internal zone 0.73-1.63 μm below the surface. Mainly AlN particles with a width of 6-30 nm and a length of 150-700 nm were present in this zone. Using high resolution TEM micrographs (Fig. 3e), the nitrides were identified as crystalline c-AlN. The AlN particles were formed intergranularly. Their presence is a clear indication of nitrogen diffusion during annealing. Fig. 4a shows the third sub-surface zone in the range of 1.63-4.0 μm below the surface. It consists of $MnAl_x$ ($x>1$) intermetallic compound particles. It is noteworthy to mention that the type and distribution of the internal oxides, and the presence of nitrides and intermetallic compounds observed in the case of CMnAl TRIP steel, are different from the observations reported in a previous study on selective oxidation of CMnSi TRIP steels by the present authors.[9),10)]

4. Discussion

Huin *et al.*[11] have proposed a general extension of Wagner's model[12] for the internal oxidation of steels which takes into account an arbitrary number of elements and oxides, and the possible formation of mixed oxides. Huin predicted that only MnO, SiO_2, Mn_2SiO_4, Al_2O_3 and MnO.Al_2O_3 can form during the selective oxidation of Al-containing CMnSi TRIP steel. His model clearly fails to predict the formation of the two distinct internal layer-type oxides and nitrides which were observed in the course of the present work. In the first zone, crystalline oxides (*c*-xMnO.SiO_2 ($1 \leq x \leq 2$) and *c*-xMnO.Al_2O_3 (x=1)) were present, and, deeper below the surface, AlN particles were observed.

The oxidation occurring during intercritical annealing is controlled by the diffusion of oxygen into the steel sub-surface. In a -24 ℃ dew point atmosphere, the oxygen diffusion is slower than the diffusion of Mn, Al and Si towards the surface and external oxidation is dominant. The selective oxidation of Mn, Al and Si then proceeds in the following three stages:

Stage 1. Mn and Si are oxidized at the surface and form the very stable mixed oxides *c*-xMnO.SiO_2 ($1x \leq 2$) and *c*-xMnO.Al_2O_3 (x=1), as the compound oxides of Mn, Al and Si have a lower Gibbs energy of formation than Al_2O_3, MnO or SiO_2. At the same time, the carbon diffuses to the surface and the decarburization takes place. Some initially formed austenite may be transformed to new ferrite due to the surface decarburization.

Stage 2. The present observations, which have revealed the internal oxidation of Mn, Al and Si to *c*-xMnO.SiO_2 (1x2) and *c*-xMnO.Al_2O_3 (x=1), suggest that oxygen diffuses through the surface oxides into the sub-surface and forms these compounds oxides.

Stage 3. The formation of the compound oxides *c*-xMnO.SiO_2 ($1 \leq x$ 2) and *c*-xMnO.Al_2O_3 (x=1) oxides results in a reduced oxygen content allowing for solute nitrogen and Al to form AlN particles.

5. Conclusions

The selective oxidation of Mn, Al and Si on the surface of a CMnAl TRIP steel intercritically annealed in gas atmosphere conditions likely to result in external oxidation (10%H_2+N_2 gas atmosphere, -24 ℃ dew point) resulted in the formation of larger crystalline *c*-xMnO.SiO_2 ($1 \leq x < 3$) and *c*-xMnO.Al_2O_3 ($x \geq 1$) oxides, small crystalline *c*-xMnO.SiO_2 (2x4) particles and a thin oxide film of crystalline *c*-xMnO.SiO_2 (2x<3) and *c*-xMnO.Al_2O_3 ($x \geq 1$) at the steel surface.

The amorphous *a*-xMnO.SiO_2 ($x \leq 0.9$) and *a*-SiO_2 oxides, which are typically formed on the surface of CMnSi TRIP steels during intercritical annealing in a low dew point atmosphere, were not observed on CMnAl TRIP steel. The amorphous *a*-xMnO.SiO_2 ($x \leq 0.9$) and *a*-SiO_2 oxides are known to have a negative effect on the wettability of the steel by liquid Zn. In addition, the formation of three separate zones of internal oxides, nitrides and intermetallic compounds was observed in the sub-surface. Although the annealing atmosphere is believed to yield conditions for external oxidation, large oxides particles consisting of 2MnO.SiO_2, MnO.SiO_2 and MnO.Al_2O_3 were formed in the sub-surface.

The low dew point atmosphere of -24 ℃ also leads to the decarburization of TRIP steel sheet surface. This decarburization and the reduction of the Mn solid solution content due to the formation of compound oxides, is believed to result in the transformation of the initial intercritical austenite to ferrite in a narrow surface region. The selective oxidation during intercritical annealing will therefore also affect the phase formation at the surface of TRIP steels.

The selective oxidation of CMnAl TRIP steel is unlikely to affect its galvanizability negatively due to the absence of amorphous *a*-xMnO.SiO_2 ($x \leq 0.9$) and *a*-SiO_2 oxides at the surface. In an earlier study of external oxidation, two oxides layers consisting of *c*-xMnO.SiO_2 ($1\ x \leq 2$) and *a*-SiO_2 were formed on the surface of CMnSi TRIP steel after intercritical annealing.[9] In the present case, no amorphous *a*-xMnO.SiO_2 ($x \leq 0.9$) or *a*-SiO_2 oxides were formed at the surface. The type of thin oxide films formed on CMnAl TRIP steel does apparently not prevent the formation of the inhibition layer when the TRIP steel sheet is immersed in the liquid Zn metal. Al-added TRIP steels, in which Si is replaced by Al, can therefore lead a good galvanizability even in external oxidation conditions.

References

1. B. C. De Cooman, *Curr. Opin. Solid State Mater. Sci*., **8**, 285 (2004).
2. J. Mahieu, S. Claessens, and B. C. De Cooman, *Metall. and Mater. Trans. A*, **32A**, 2905 (2001).
3. J. Mahieu, S. Claessens, B. C. De Cooman, and F. Goodwin, Proceedings of the 6th International Conference on Zinc and Zinc Alloy Coated Steel Sheet (Galvatech), M.A. Baker Editor, Association for Iron and Steel Technology, p. 529, Chicago, Illinois, (2004).
4. C. Ramadeva Shastry, John A. Rotole, and Thomas W. Kaiser, Proceedings of the 7th International Conference on Zinc and Zinc Alloy Coated Steel Sheet (Galvatech), Association for Iron and Steel Technology, p. 403, Osaka, Japan, (2007).
5. B.R. Strohmeier and D. M. Hercules, *J. Phys. Chem*., **88**, 4922 (1984).
6. E.M. Bellhouse, A.I.M. Mertens, and J.R. McDermid, *Mater. Sci. Eng. A*, **463**, 147 (2007).
7. X. Vanden Eynde, J. P. Servais, and M. Lamberigts, *Surf. and Inter. Ana.*, **35**, 1004 (2003).
8. Y.F. Gong, S. Birosca, Han S. Kim, and B. C. De Cooman, *J. Microscopy*, **230**, 424 (2008).
9. Y.F. Gong, Han S. Kim, and B. C. De Cooman, *ISIJ Int.*, **48**, 1745 (2008).
10. Y.F. Gong, Han S. Kim, and B. C. De Cooman, *ISIJ Int.*, **49**, 557 (2009).
11. D. Huin, P. Flauder, and J. B. Leblond, *Oxidation of Metals*, **64**, 132 (2005).
12. C. Wagner, Z. Elektrochemie, **63**, 772 (1959).
13. J. Mahieu, Doctoral Thesis, p. 79, Ghent University, Ghent, Belgium (2006).